Thesis for the Degree of Master of Science

Study on the effect of an aspect ratio on air quality in urban street canyons

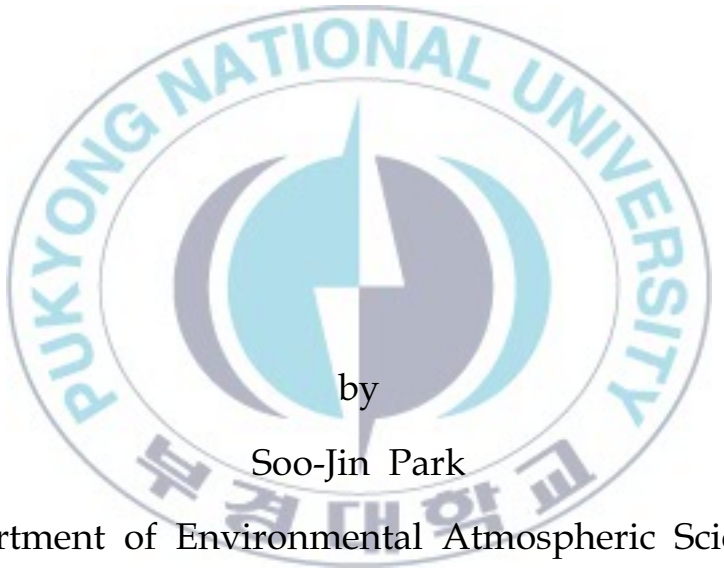

by

Soo-Jin Park

Department of Environmental Atmospheric Sciences

The Graduate school

Pukyong National University

February 2013

Study on the effect of an aspect ratio on air quality in urban street canyons

도시협곡 외관비에 따른 대기질 특성 연구

Advisor: Prof. Jae-Jin Kim

by

Soo-Jin Park

A thesis submitted in partial fulfillment of the requirements
for the degree of

Master of Science

in Department of Environmental Atmospheric Sciences, the Graduate School
Pukyong National University

February 2013

Study on the effect an aspect ratio on air quality in urban street canyons

A dissertation

by

Soo-Jin Park

Approved by:

(Chairman) Byoung-Hyuk Kwon

(Member) Hyeong-Bin Cheong

(Member) Jae-Jin Kim

February 22, 2013

Contents

List of Figures

List of Tables

도시 협곡 외관비에 따른 대기질 특성 연구

박 수 진

부 경 대 학 교 대 학 원 환 경 대 기 과 학 과

요 약

본 연구에서는 CFD-Chem 모델을 이용하여 도시 협곡 외관비가 도시 협곡 내의 대기질 특성에 미치는 영향을 분석하였다. CFD-Chem 모델은 화학반응에 대하여 Gear 방식의 Solver 를 사용하고 광화학 반응 계수 산출을 위하여 Fast-J 모듈을 이용하여 화학반응에 적용한다. 모델 도메인의 경우 무한히 반복되는 건물 군을 가정하였으며 건물의 높이, 건물의 길이, 도로 협곡의 너비를 변화하여 외관비 변화를 고려하였다. 배출은 NO_x 에 대하여 협곡의 중심에서 선 오염원을 가정하고, 87가지의 화학 물질에 대하여 배경 농도를 적용하였다. 반응성 오염물질의 확산에 영향을 줄 수 있는 도시 협곡 외관비 변화에 따른 흐름장을 분석하였고, 도심 지역의 주요 오염 물질인 NO, NO_2, O_3 에 대하여 농도 분포 특성을 분석하였다. 건물 높이 변화에 따라 협곡 내에서 2차 순환 (the secondary vortex)이 발생하고, 2차 순환이 나타나는 지역에서 높은 농도의 NO, NO_2 가 나타났다. O_3 의 경우, NO에 의한 O_3 소멸로 인하여 NO_x 의 농도가 높은 2차 순환이 나타나는 지역에서 낮은 농도의 O_3 분포가 나타났다. 건물 너비 변화의 경우, 건물의 너비가 증가할수록 협곡 내부로 향하는 흐름이 증가하고, 이는 도시 협곡의 중심에서 NO와 NO_2 의 농도가 높게 나타나는 원인이 되었다. 협곡의 중심에서 높은 농도의 NO와 NO_2 분포는 도시 협곡의 중심에서 낮은 농도의 O_3 분포를 야기하였다. 도로 협곡 너비 변화의 경우, 도로 협곡 너비의 증가는 협곡 내부의 흐름 체계 (flow regime)에 영향을 주는 원인이 되었다. 풍상측 건물 후면에 이중 에디 순환이 발생하는 경우, 풍상측 건물 후면에서 협곡 외부로 향하는 흐름을 방해하여 풍상측 건물 후면에 높은 농도의 NO 와 NO_2 가 나타났다. O_3 의 경우, 도로 협곡 너비가 증가할수록 협곡 내부로 유입되는 O_3의 양이 증가하여 풍하측 건물 부근에서 높은 농도의 O_3 분포가 나타났고, NO와 NO_2 농도가 높은 풍상측 건물 부근에서 O_3 농도가 낮게 나타났다. 이와 같이, 도시 협곡 외관비 변화는 협곡 내에서 다양하고 복잡한 흐름 변화를 가져오고, 이는 배출 물질인 NO 와 NO_2 의 확산에 영향을 주었다. 또한, NO_x 는 O_3 의 생성·소멸 반응에 관여하여 O_3 의 농도 분포에 영향을 주었다.

Ⅰ. Introduction

The population in urban area increased recently with the persistent urbanization. Pollutants on increase of energy consumption and traffic vehicles cause damage to human being. Also, a primary and secondary pollution exceed the standard in major cities. Therefore, over the years, flow and dispersion in urban area have been investigated with the increase of concern for air pollution. Most of the previous studies mainly focus on dynamical processes and unreactive pollutant dispersion in microscale model (Assimakopoulos *et al.*, 2003; Baik *et al.*, 2009; Kim and Baik, 2004; Liu *et al.*, 2002; Sagrado *et al.*, 2002). However, the pollutants emitted in urban area are mostly reactive pollutants such as NO_X and O_X. To understand the flow and reactive pollutants dispersion and to better predict them in urban area, a high-resolution grid system are required. Accordingly, coupled model for microscale model and the chemistry model used to analyze the flow and reactive pollutants dispersion on microscale (Baik *et al.*, 2007; Kang *et al.*, 2008; Kwak *et al.*, 2012). Coupled model with microscale model can be the high-resolution calculation and specifically can be analyze the flow and reactive pollutants dispersion on microscale. Therefore, recent studies have focused on reactive pollutant dispersion in urban area using the coupled model for microscale model and chemistry model (Garmory *et al.*, 2009; Kikumoto *et al.*, 2012; Kim *et*

al., 2012; Kwak *et al*., 2012). CFD-Chem model used to simulate the dispersion of reactive pollutants in the street canyon. It has been include in reactions and transport of chemical species such as NO, NO_2, and O_3 with the steady state photochemistry (Baker *et al*, 2004; Baik *et al*., 2007; Kim *et al*., 2012; Liu *et al*, 2004). For example, Garmory *et al*. (2009) investigated the effect of segregation on reactive pollution using field Monte Carlo method in the street canyon. They found that the variance of reactive scalars such as NO_2 was very high in mixing region, and that the effect of segregation on major species such as O_3 was found to very small. Kwak *et al*. (2012) examined the O_3 sensitivity to the NO_X and VOC emission levelin street canyon. They found that concentration of NO_2 and O_3 emission level reduced as NO_X emission level increases in the street canyon than above it, in contrast, concentration of NO_2 and O_3 reduced as VOC emission level increases in the street canyon than above it.

Obstacle aspect ratio in downtown area mainly effects on microscale flow. Also, the dispersion in urban street canyon is effected by the aspect ratio of the street canyon (Chan *et al*., 2002; Cheng *et al*., 2003; Mukherjee and Viswanathan, 2001; Li *et al*., 2008; Park *et al*., 2004). For example, Park *et al*. (2004) examined the dispersion of vehicle emission on aspect ratio and wind direction in the street canyon. They found that the increase of the W/H ratio decreases the pollutant concentration and that the pollutant concentration in leeward

was higher than in windward. Li *et al* (2008) investigate the effect of aspect ratio on flow and dispersion using the large-eddy simulation with a one-equation subgrid-scale model. They found that strength inside the street canyon decreased as building height decreased. It suggested that aspect ratio in urban street canyon have an effect on reactions and dispersion of pollutants.

In this study, the effects of an aspect ratio on air quality in urban street canyons are investigated systematically and simulate flow and reactive pollutant dispersion using the CFD-Chem model.

This paper consists of four sections. Background and necessity of the study are given the above section. In section 2, the CFD-Chem model description and simulation setup are described. In section 3, the simulation results are discussed. A summary and conclusion are presented in section 4.

Ⅱ. Numerical experiment

1. Numerical model

The computational fluid dynamics (CFD) model includes a three-dimensional, nonhydrostatic, nonrotating, incompressible air flow system. The model is the Reynolds-average Navier-Stokes equation model (Kim and Baik, 2004) with the renormalization group (RNG) k-ε turbulence scheme that proposed by Yakhot *et al* (1992). This scheme differs from the standard k-ε turbulence scheme in that it includes an additional sink term in the turbulence dissipation equation to account for nonequilibrium strain rates and employs different values for the model coefficients (Tutar and Oquz, 2002).

The GEOS-Chem model used for chemical model is a global 3-D chemical transport model (CTM) for atmospheric composition driven by meteorological input from the Goddard Earth Observing System (GEOS). Convective transport in GEOS-Chem is computed from the convective mass fluxes in the meteorological archive, as described by Wu *et al* (2007). Boundary layer mixing in GEOS-Chem uses the non-local scheme of Lin and McElroy (1996). Also, the model includes detailed HO_X-NO_X-VOC-ozone tropospheric chemistry as originally described by Bey *et al.* (2001a).

The CFD-Chem model used in this study is coupled model for CFD model and GEOS-Chem model. A full tropospheric NO_X-O_X-VOCs chemical mechanism from GEOS-Chem is coupled with the CFD model. The chemical scheme includes 110 species and 343 reactions among which 50 reactions are photochemical reactions. The chemical computation is done using a gear type solver, Sparse Matrix Vectorized Gear Code (SMVGEAR) (Jacobson and Turco, 1994) that has been used in global and regional chemical models. The SMVGEAR is used for solve gas-phase and size bin-resolved aqueous-phase chemistry in an air pollution model that also computes the effects of many other processes.

The Fast-J algorithm used to calculate the photolysis rate coefficients (Wild *et al.*, 2000). The algorithm is sufficiently fast to allow the scheme to be incorporated into 3-D global chemical transport models and have photolysis rates updated hourly. The scheme may also be used to calculate short-wave heating rates without requiring additional computational resources. Also, the scheme uses in real-time the physics predicted in each model layer and can easily add new photolysis rates at negligible cost.

2. Experimental setup

Figure 1 shows the computational domain and building configuration used in the current study. The computational domain consists of the group of buildings that repeated infinitely in x- and y-direction. A main concern in this study is to investigate the effect of an aspect ratio on air quality in urban street canyon. For the symmetric variation of street aspect ratio in the computational domain, building height (H = 20 m, 30 m, 40 m, 50 m), building width (W = 20 m, 30 m, 40 m, 50 m), street width (S = 20 m, 30 m, 40 m, 50 m) give numerical experiments. The maximum domain sizes (cell number) are 190 m × 60 m × 200 m (95 × 30 × 100) and the minimum domain sizes (cell number) are 100 m × 60 m × 200 m (50 × 30 × 100) in x-, y-, and z-directions, respectively. The grid interval of all sorts of the domain is 2 m in the x-, y-, and z-direction. The building and street width sizes of control case are 20 m in building height, 20 m in building width, 20 m in street width. Table 1 indicates the detailed experimental descriptions about street aspect ratio for ten-case in urban street canyon. The vertical profiles of ambient wind, turbulent kinetic energy and its dissipation rate are as follows (Castro and Apsley, 1997) :

$$U(z) = \frac{U_*}{\kappa} \ln\left(\frac{z}{z_0}\right)\cos\Theta \quad (1)$$

$$V(z) = \frac{U_*}{\kappa} \ln\left(\frac{z}{z_0}\right)\sin\Theta \quad (2)$$

$$W(z) = 0 \quad (3)$$

$$k(z) = \frac{U_*^2}{C_\mu^{1/2}}\left(1 - \frac{z}{\delta}\right)^2 \quad (4)$$

$$\varepsilon(z) = \frac{C_\mu^{3/4} k^{3/2}}{\kappa z} \quad (5)$$

Where U_*, Θ, z_0, δ, and κ are the friction velocity, wind direction, roughness length (= 0.05 m), the boundary layer depth (= 1000 m), von Karman constant (= 0.4), respectively. C_μ is an empirical constant (= 0.0845). The ambient wind speed is 3 m s^{-1} at rooftop level (20 m). The air temperature is set to be 308 K (isothermal condition).

The CFD-Chem model with a full chemistry mechanism is integrated for 90 min with a time step of 0.1 s. For the first 30 min (t = 0 ~ 30 min) of model integration, there are no emissions for NO and NO_2 in order to establish a primary vortex within the street canyon and the turbulent wind fields in domain. After t = 30 min, passive pollutants are emitted at a rate of 50 and 5 ppbvs^{-1} per grid cell for NO and NO_2, respectively. The emissions of NO_X are separated

into NO and NO_2 emissions using 10:1 ratio by volume, following the method in Baker *et al.* (2004). The concentration of initial O_3 is assumed to be 20 ppbv. The emission source in the computational domain is located in the center of the street canyon (4 grid cell wide (8 m)) and the each grid cell of the lowest model level (z = 2 m) (Fig 1). In this study, the flow and dispersion of NO, NO_2, and O_3 are analyzed as aspect ratio in urban street canyon.

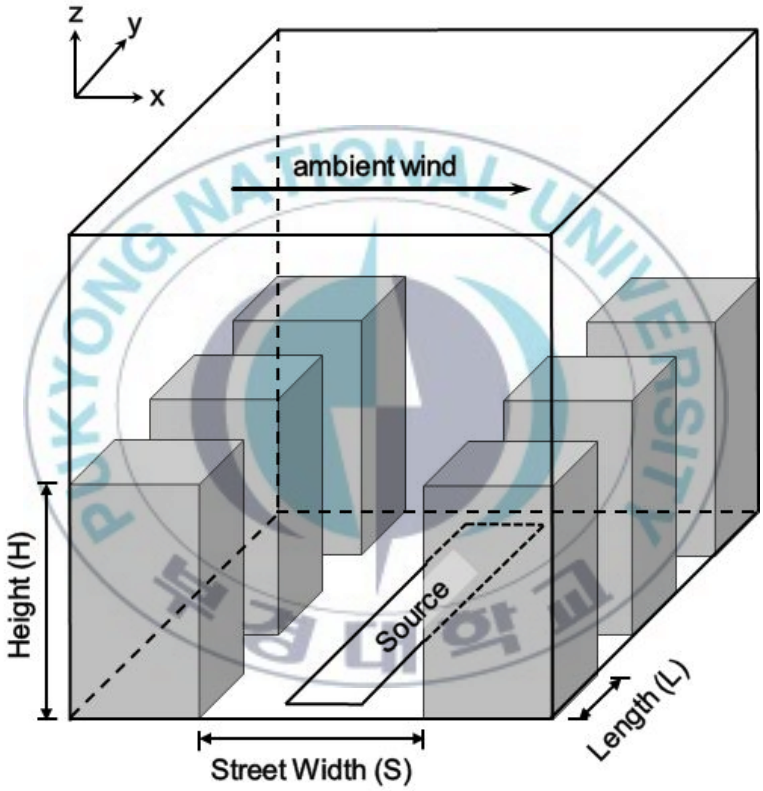

Fig. 1. The computational domain and building configuration.

Table 1. Summary of experimental designs.

Experiments	Building Height (m)	Building Length (m)	Street Width (m)
CTRL	20	20	20
Exp_H1	**30**	20	20
Exp_H2	**40**	20	20
Exp_H3	**50**	20	20
Exp_L1	20	**30**	20
Exp_L2	20	**40**	20
Exp_L3	20	**50**	20
Exp_S1	20	20	**30**
Exp_S2	20	20	**40**
Exp_S3	20	20	**50**

Ⅲ. Results and Discussion

The dispersion of NO, NO_2, and O_3 in the street canyons using the simple photochemistry investigated by Baker *et al.* (2004) and Garmory *et al.* (2009). Baker *et al.* (2004) examined the dispersion using the simple photochemistry and NO, NO_2, and O_3 concentrations calculated. However, they did not consider the aspect ratio in the street canyon and the three-dimensional domain. The three-dimensional domain forms complexity flows in the street canyon because the flow blows inward and outward on both sides of the street canyon. In three-dimensional domain, the spiral flows, a portal vortex, appear in the street canyon (Kim *et al.*, 2010). Also, as mentioned earlier, the aspect ratio effects on flow and dispersion in the street canyon.

The most of simulation results are discussed with the simplified general photochemical reactions, even thought photochemical reactions of the atmospheric is more complicated. The photochemistry oxidants such as O_3 are generated by chemical reactions involving solar ultraviolet rays and its emission of primary pollutants such as NO_X and RH in the atmosphere. The simplified general photochemical reactions are as follows (Kim *et al.*, 2008) :

$$NO_2 + h\nu + O_2 \rightarrow NO + O_3 \quad (6)$$

$$RH + OH + O_2 \rightarrow RO_2 + H_2O \quad (7)$$

$$CO + OH + O_2 \rightarrow HO_2 + CO_2 \quad (8)$$

$$RO_2 + NO + O_2 \rightarrow RCHO + HO_2 + NO_2 \quad (9)$$

$$HO_2 + NO \rightarrow OH + NO_2 \quad (10)$$

$$O_3 + h\nu + H_2O \rightarrow 2OH + O_2 \quad (11)$$

$$NO + O_3 \rightarrow NO_2 + O_2 \quad (12)$$

$$HO_2 + O_3 \rightarrow OH + 2O_2 \quad (13)$$

$$OH + NO_2 \rightarrow HNO_3 \quad (14)$$

Here, O_3 production results from photolysis of NO_2. The decreasing of NO_2 lead to a decrease in O_3 production (6). RO_2 is produced by reactions of OH with RH in (7), and leads to the decreasing of HO_2 in (9). Also, HO_2 is produced by reactions of OH with CO in (8). NO_2 production is decreased as reaction of HO_2 with NO decreases in (10). The removal of O_3 results from photolysis, reaction (11), and reactions with NO and HO_2, reactions (12) and (13). Also, formation of HNO_3 is important for removal of O_3 in (14).

In this study, the reactive gases investigated are NO and NO_2 emitted into the street canyon by traffic using the CFD-Chem model with a full chemistry mechanism. The dispersion of NO, NO_2, and O_3 examines with an aspect ratio of street canyon in three-dimensional domain. For understanding of the flow pattern and the pollutant distribution in urban street canyons, the wind vector fields (horizontal and vertical) and the vertical concentration distribution of reactive pollutants are investigated. Also, NO, NO_2, and O_3 concentrations were used to investigate trend of the concentration in the street canyon.

1. The effects of building height

Figure 2 shows the fields of horizontal wind vectors in the street canyon with the change of building height (= 20 m, 30 m, 40 m, 50 m). The wind speed increases as building height increases in the streamwise (x-direction) street canyon due to the channeling effects. In the case of CTRL and Exp_H1, the reverse flows appear near the bottom. The wind blows upward and outward around the upwind building wall. Also, the wind blows downward and outward around the downwind building wall near the bottom. In the case of Exp_H1, reverse flow weak near the bottom, and the outward flow appears more intensively than that of CTRL case (Fig. 2b). In the case of Exp_H2 and Exp_H3, the wind blows from upward building to downward building near the bottom, in contrasted with the case of CTRL and Exp_H1. The wind blows downward and outward around the upwind building wall. Also, the wind blows upward and inward around the downwind building in the lower layer. These flow patterns are also ascertained from vertical wind vector fields (Fig. 3). The vertical cross sections show that the vortex forms in the street canyon. In the case of CTRL and Exp_H1, one clockwise-rotating vortex is generated in vertical cross section and reverse flow appears near the bottom (Figs. 3a and 3b). In the case of Exp_H2 and

Exp_H3, the primary vortex, clockwise-rotating, is generated in the upper layer, and the secondary vortex, counterclockwise-rotating, is formed in the lower layer. The center of the secondary vortex moves to around the upwind building wall with the increase of building height. Also, the reverse flow does not appear near the bottom due to the counterclockwise-rotating vortex in a street canyon (Figs. 3c and 3d). On the other hand, in the tall street canyon, two counter rotating vortices effect on the flow in the street canyon.

From the above results, the different flow patterns appear in the street canyon as building height varies. It is show that the flow patterns in the street canyon depend on the vertical vortex forms and the rotating direction of vortex.

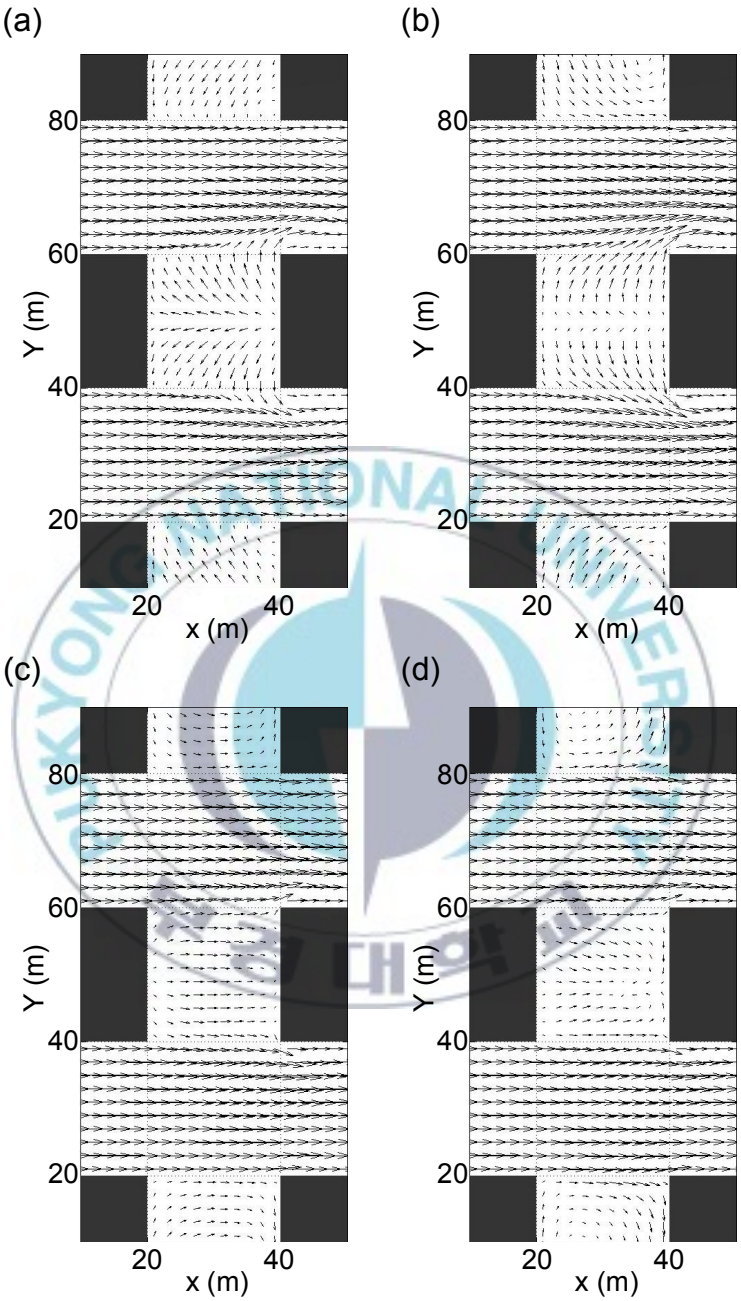

Fig. 2. The fields of horizontal wind vector at h = 1 m in the case of (a) CTRL case, (b) Exp_H1 case, (c) Exp_H2 case and (d) Exp_H3 case.

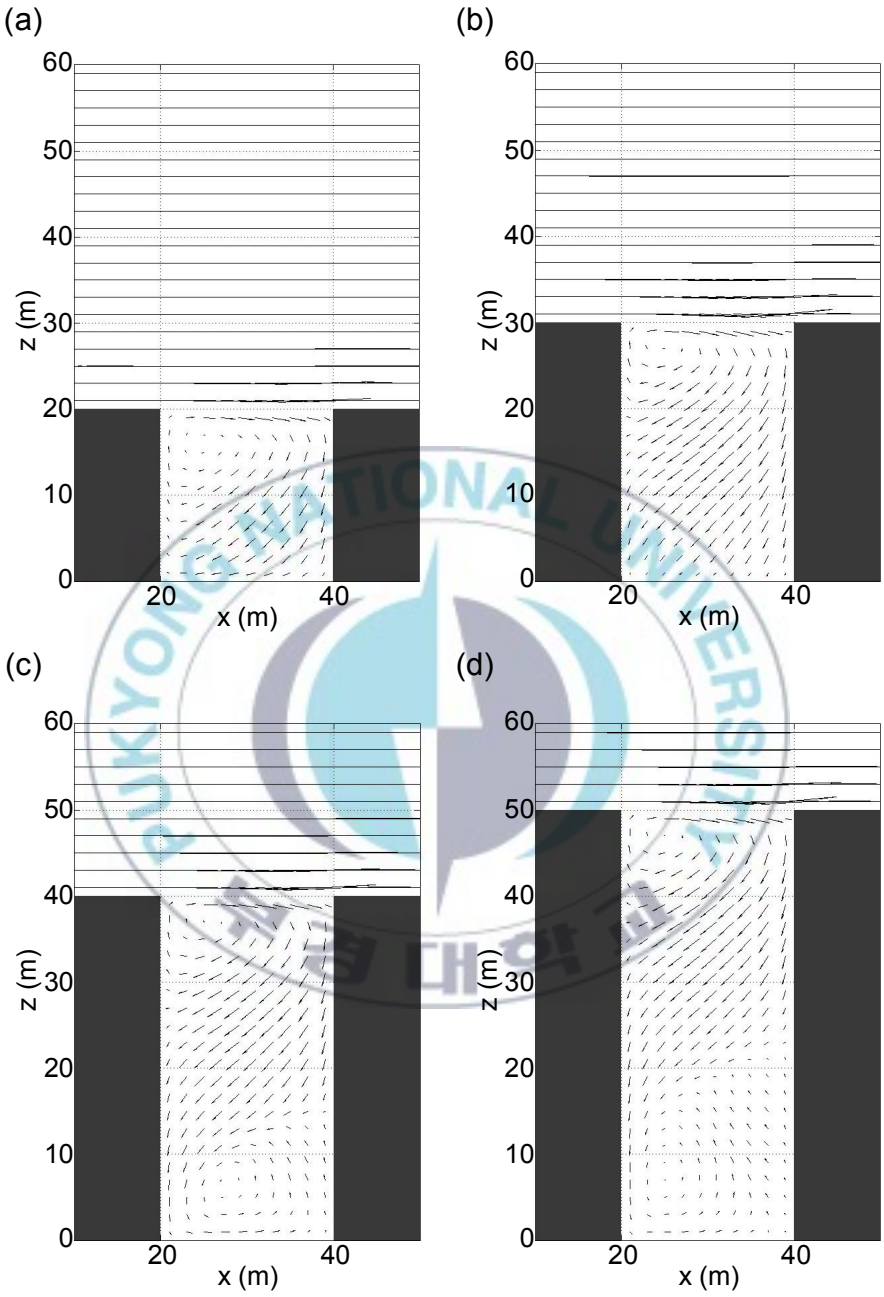

Fig. 3. The fields of vertical wind vector in the case of (a) CTRL case, (b) Exp_H1 case, (c) Exp_H2 case and (d) Exp_H3 case.

Four numerical simulations are performed with the change of building height and the simulation results for the dispersion of the reactive pollutant are analyzed. Figure 4 and 5 shows NO and NO_2 concentrations fields with the change of building height, respectively. In the case of CTRL, the concentration distribution of NO appears along the primary vortex in the street canyon. NO concentration at the leeward side is higher than at windward side because of the reverse flows. The maximum concentration of NO appears in the center of the street canyon. NO concentration is broadly high 150 ppbv around the center of the street canyon near the bottom. The concentration distribution of NO_2 appears to be similar that of NO, but concentration around center of the street canyon is about 15 ppbv. In the case of the Exp_H1, NO concentration at the leeward side is similar to be that at the windward side. Because the reverse flows are weak near the bottom, the wind blows outward in the street canyon (Fig. 2b). In the case of Exp_H2 and Exp_H3, NO and NO_2 concentrations are lower at the leeward side than at windward side in the lower layer. Also, NO and NO_2 concentrations in the case of Exp_H2 and Exp_H3 are higher than that of CTRL and Exp_H1 because wind speed decreases at the region where the secondary vortex appears. The secondary vortex in the street canyon generates the stagnation of NO and NO_2 in lower layer, and it leads to higher NO and NO_2 concentrations. The maximum concentration of NO in Exp_H2 case appears around the

downward building, but the maximum concentration of NO in Exp_H3 case appears around the center of street canyon in the lower layer. The center of counterclockwise-rotating vortex located around the middle of street canyon generates the upward motion around the downward building (Figs. 3c). However, the center of counterclockwise -rotating vortex located around the upward building generates the upward motion around the center of the street canyon (Figs. 3d). Figure 6 shows O_3 concentration fields with the change of building height. O_3 is entrained into the street canyon along the downward building wall. Following the primary vortex in CTRL case, O_3 concentration is lower than 20 ppbv in the street canyon. In the case of CTRL and Exp_H1, O_3 concentration is the highest at the center of vortex in contrasted with NO and NO_2 concentrations. These patterns are shown consistently in other modeling studies (Baik *et al.*, 2007; Baker *et al.*, 2004). In the case of Exp_H2 and Exp_H3, NO and NO_2 are entrained into the upper along the upward building wall while O_3 is entrained into the street canyon along the downward building wall at rooftop level. O_3 concentration is higher at the upper layer than at the lower layer. The lowest concentration of O_3 is shown at the region where the secondary vortex is generated because O_3 concentration is depleted by the NO titration of O_3.

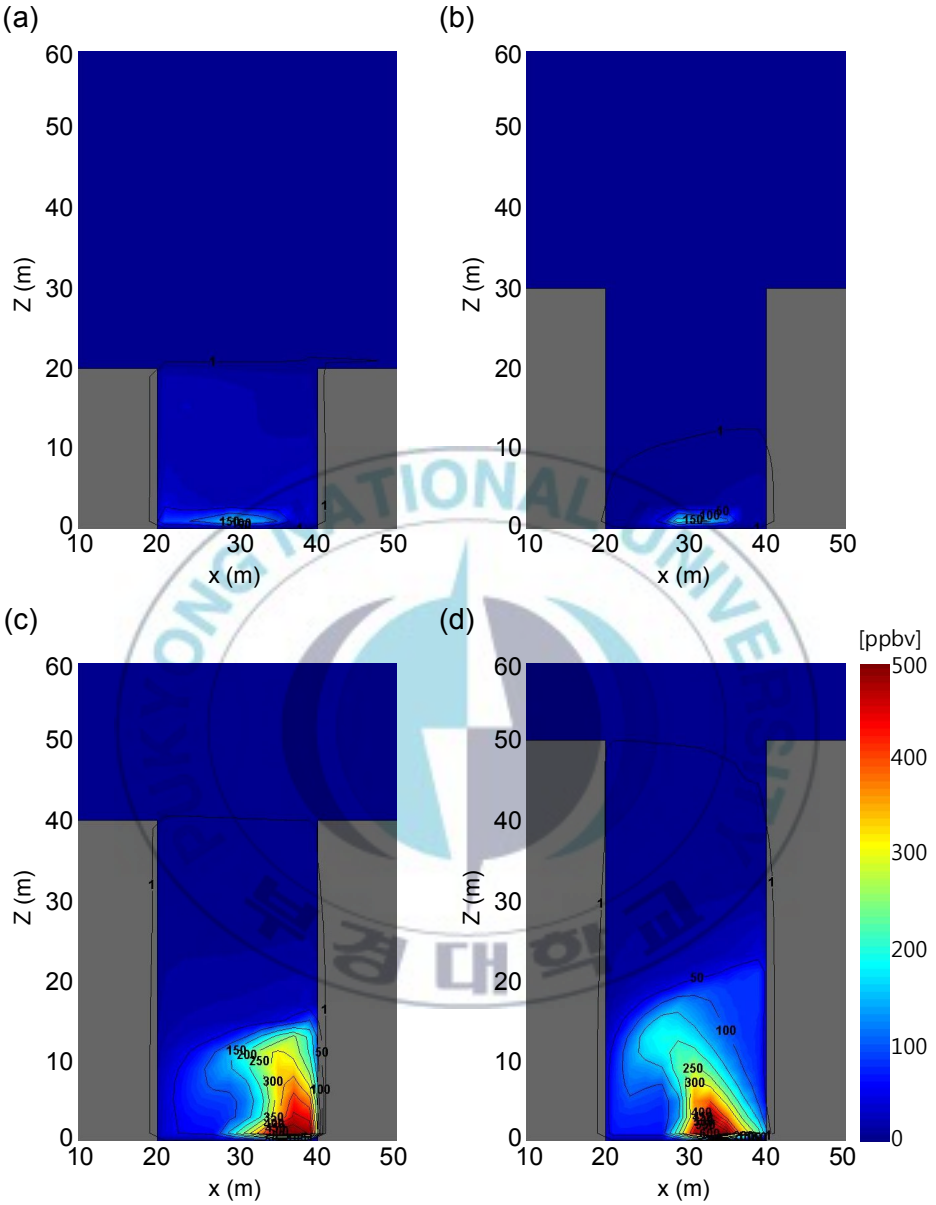

Fig. 4. NO concentration fields along the street canyon axis in the case of (a) CTRL case, (b) Exp_H1 case, (c) Exp_H2 case and (d) Exp_H3 case.

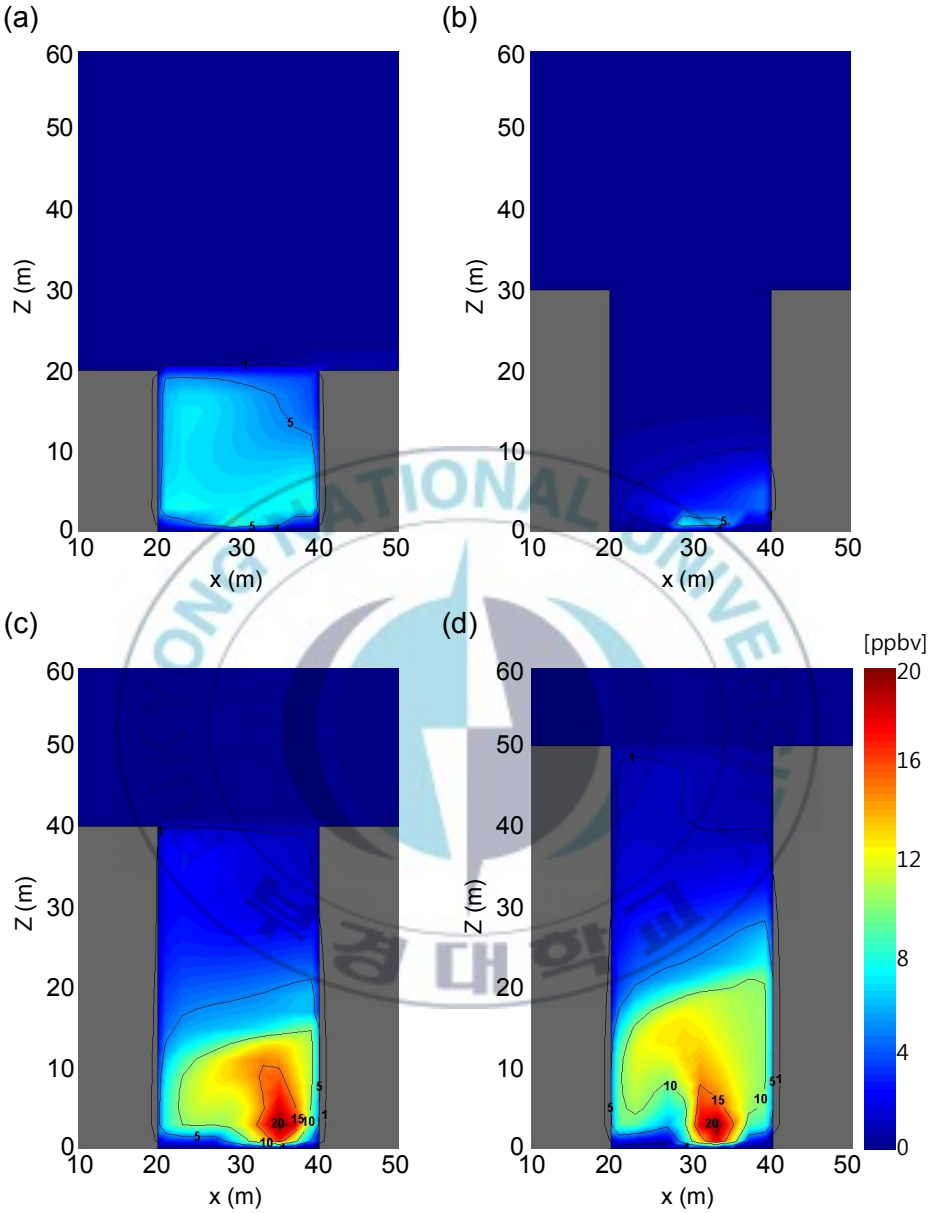

Fig. 5. NO_2 concentration fields along the street canyon axis in the case of (a) CTRL case, (b) Exp_H1 case, (c) Exp_H2 case and (d) Exp_H3 case.

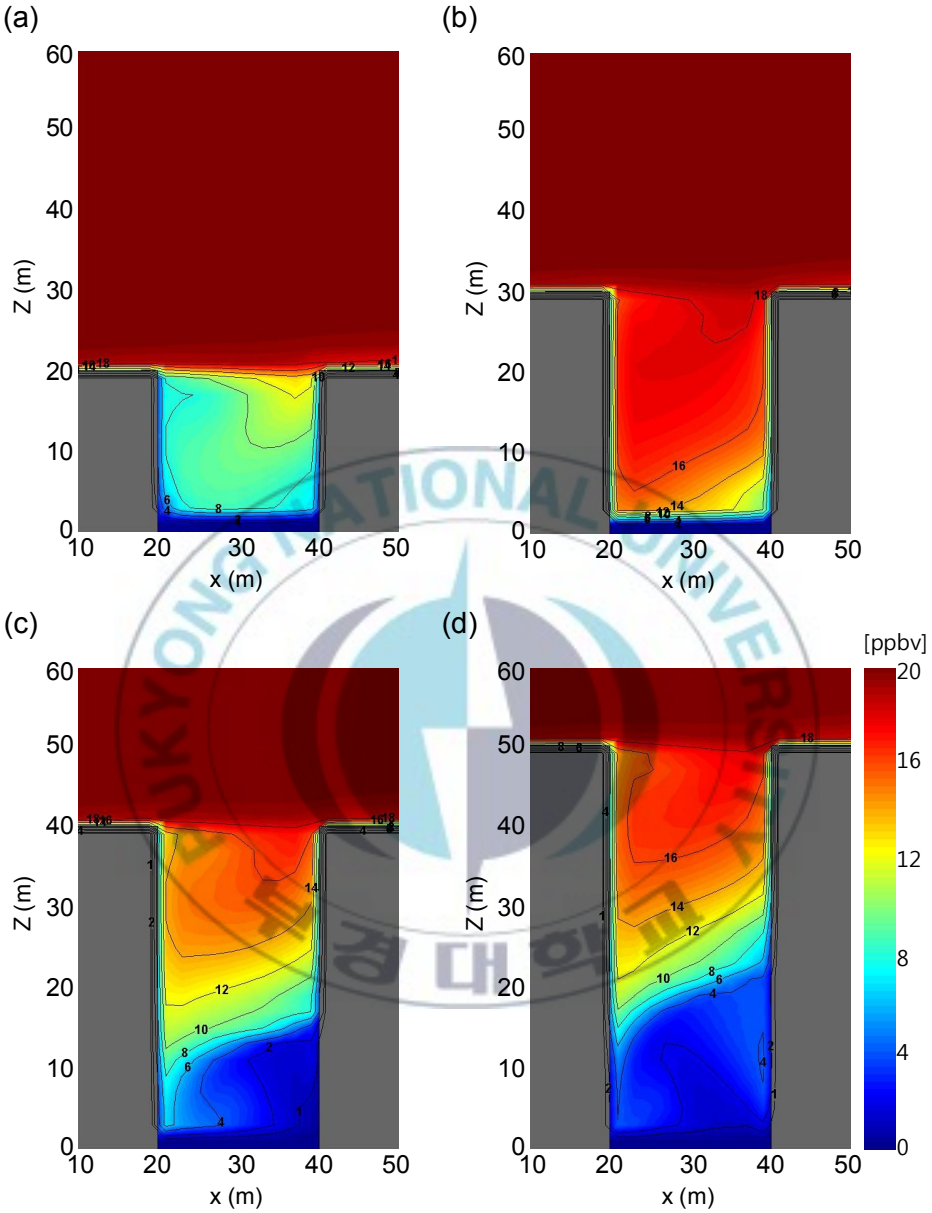

Fig. 6. O_3 concentration fields along the street canyon axis in the case of (a) CTRL case, (b) Exp_H1 case, (c) Exp_H2 case and (d) Exp_H3 case.

Figure 7 shows the average concentration of NO, NO_2, and O_3 ar the bottom (z = 2 m) and at the whole street canyon with the change of building height. The average concentration at the whole street canyon considers the volume for each cases. NO and NO_2 concentrations increase as building height increases at the bottom and the whole street canyon except for Exp_H1 case because of the outward flow in the street canyon. NO and NO_2 concentrations are the highest in Exp_H3 case. The pattern of NO_2 concentration is similar to that of NO, but NO_2 concentration is almost uniform. The pattern of O_3 concentration is contrasted with that of NO and NO_2. The average concentration of O_3 at the whole street canyon is relatively higher than at the bottom because NO concentration is lower than near at bottom.

Figure 8 shows the average concentration of NO, NO_2, and O_3 at the leeward side and at the windward side with the change of building height. The leeward side expresses the area from upward building wall to the center of canyon. The windward side expresses the area from the center of canyon to downward side wall. Also, the average concentration consider the volume for each cases. In the case of CTRL, the average concentration of NO and NO_2 at the leeward side is higher than at the windward side because of the reverse flow at the bottom. In the case of Exp_H1, Exp_H2, and Exp_H3, the average concentration of NO and NO_2 is higher at the windward side than at

the leeward side. The average concentration of NO and NO_2 at windward side in Exp_H2 case is higher than in Exp_H3 case because of the position of the vortex core. The average concentration of O_3 is contrasted with that of NO and NO_2. The difference of O_3 concentration between at the leeward side and at the windward side is relatively low than that of NO and NO_2.

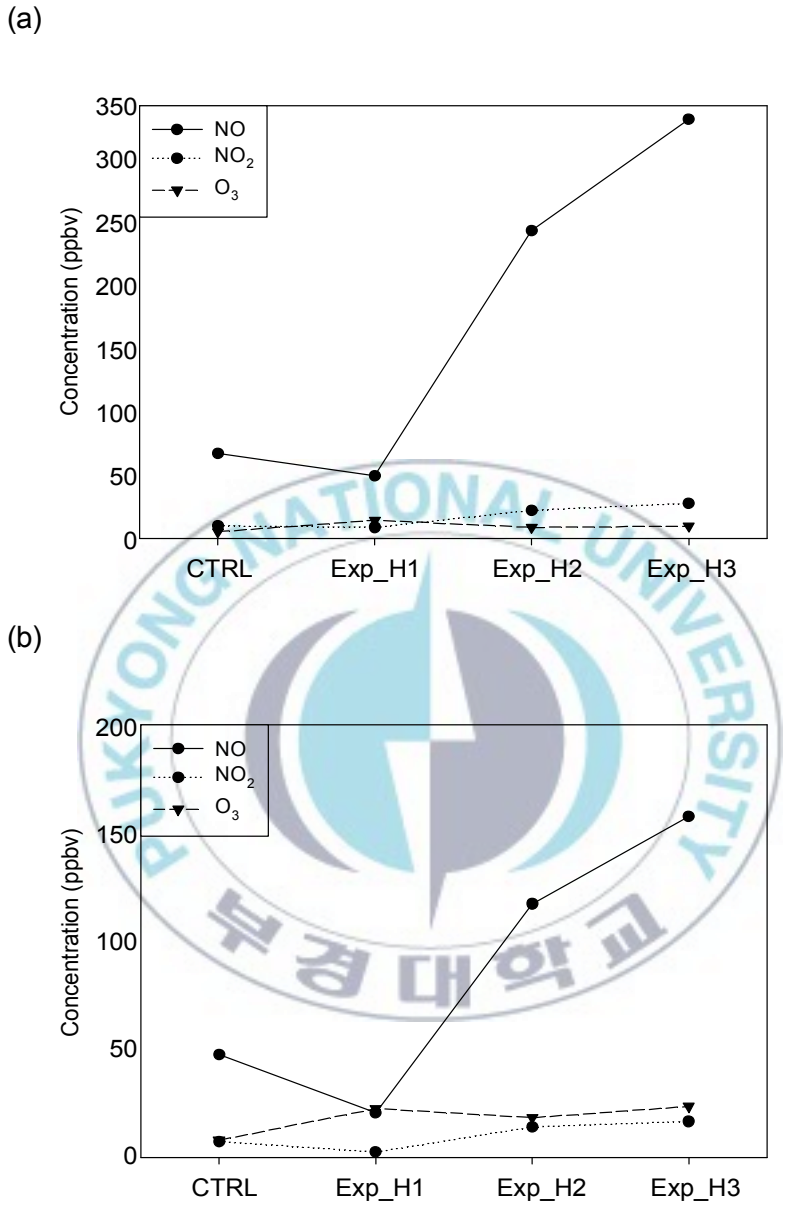

Fig. 7. The mean concentration of NO, NO_2 and O_3 (a) near the bottom in the street canyon and (b) at the whole street street canyon with the change of building height.

(a)

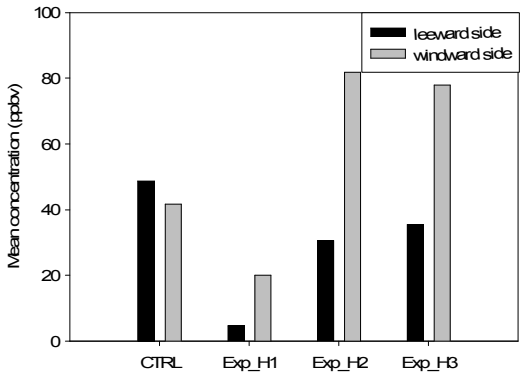

(b)

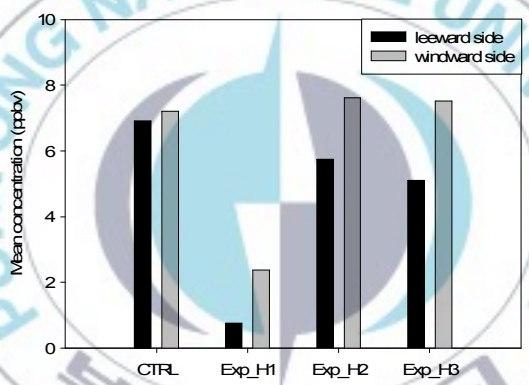

(c)

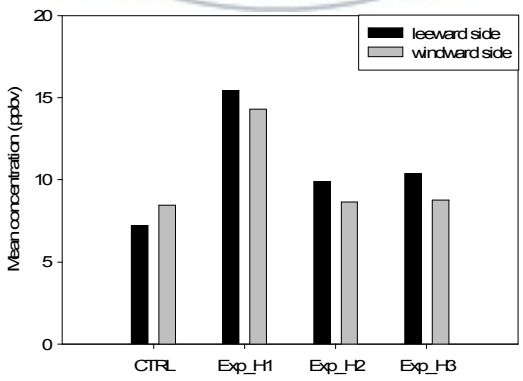

Fig. 8. The mean concentration of (a) NO, (b) NO_2, and (c) O_3 at the leeward side and at the windward side with the change of building height.

2. The effects of building length

Figure 9 shows the fields of horizontal wind vectors in a street canyon with the change of building length (= 20 m, 30 m, 40 m, 50 m). In all the four cases with the change of building length, the reverse flows appears near the bottom due to the clockwise-rotating vortex in the street canyon. The wind blows upward and outward around the upwind building in the lower layer. The wind blows downward and outward around the downwind building in the lower layer except for the case of Exp_L3. The intensity of outward flows in the street canyon decreases as building length increases. In the case of Exp_L2 and Exp_L3, the double-eddy circulation appears around the both sides of the downwind building. The magnitude of the double-eddy circulation is extended around the center of the street canyon as building length increases (Figs. 9c and 9d). The flows are converged to the center of the street canyon. Accordingly, the wind blows downward and inward around the downwind building in the lower layer.

Figure 10 shows the fields of vertical wind vectors in the street canyon. The vertical cross sections show that one clockwise-rotating vortex forms in the street canyon. It is ascertain that the reverse flows appear near the bottom due to the one clockwise-rotating vortex. In the case of CTRL, the stagnation point is generated around

the rooftop level of upward building. In the case of Exp_L3, the stagnation point appears around the edge of downwind building in rooftop level. It is found that the center of the vortex in the street canyon moves from upward building wall to downward building wall in the rooftop level.

From the above results, the change of building length effects on the flow patterns in the street canyon. The flow patterns in the street canyon depend on the existence of the double-eddy circulation around the downward building and the center of vertical vortex.

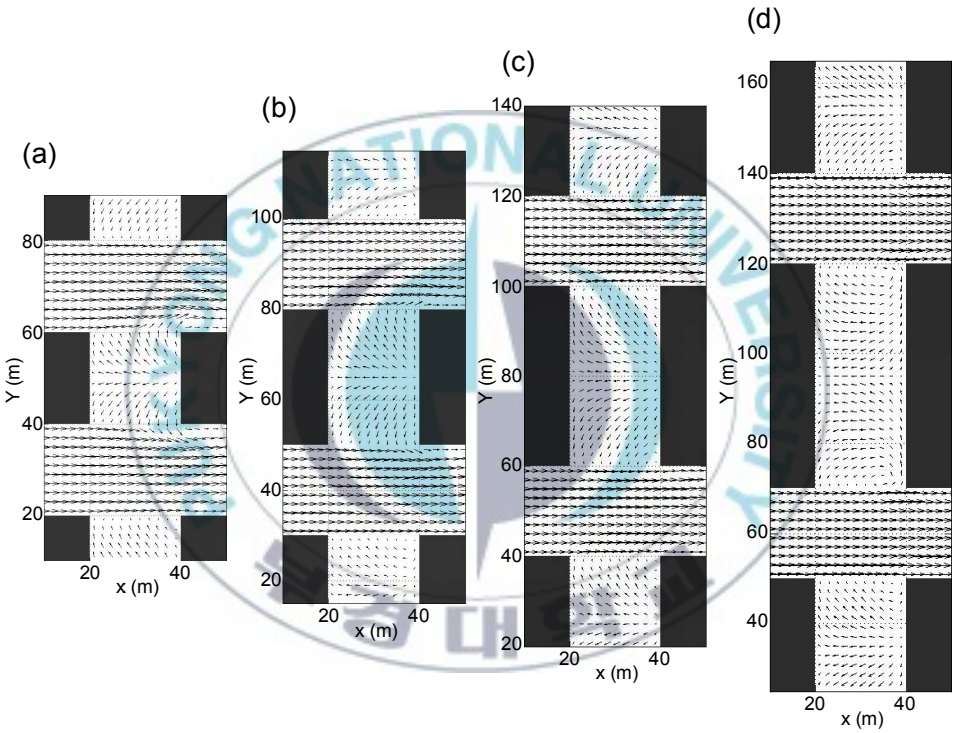

Fig. 9. The fields of horizontal wind vector at h = 1 m in the case of (a) CTRL case, (b) Exp_L1 case, (c) Exp_L2 case and (d) Exp_L3 case.

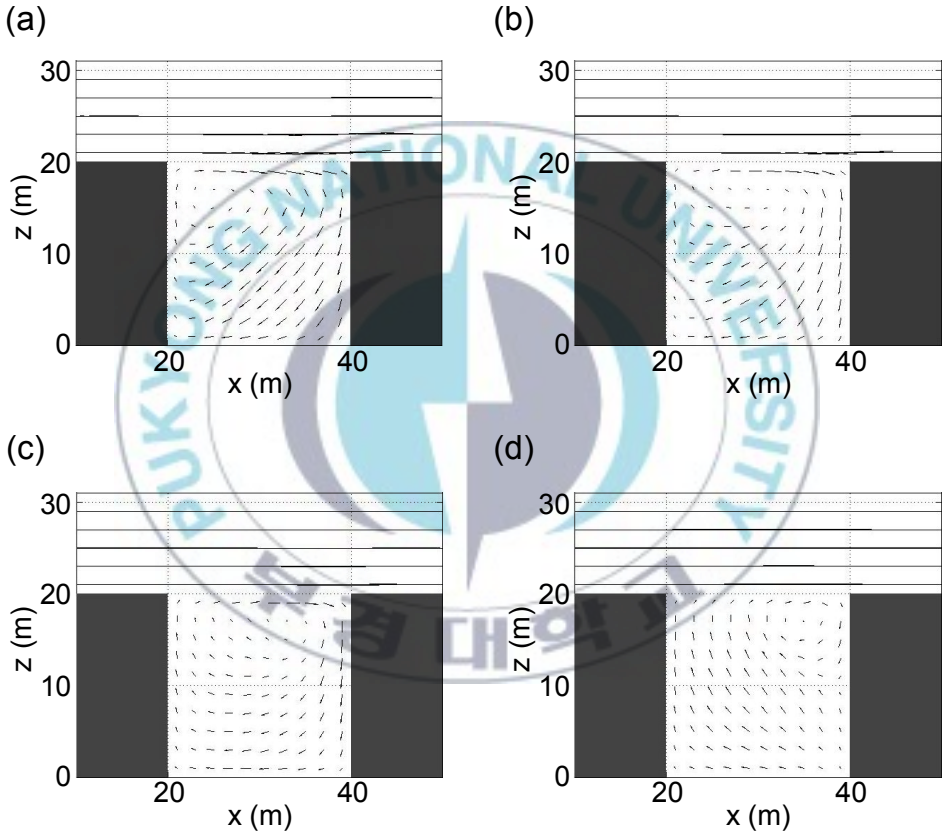

Fig. 10. The fields of vertical wind vector in the case of (a) CTRL case, (b) Exp_L1 case, (c) Exp_L2 case and (d) Exp_L3 case.

Four numerical simulations are performed with the change of building length and the simulation results for the dispersion of the reactive pollutant are analyzed. Figure 11 shows NO concentration fields with the change of building length. In all the four cases with the change of building length, the concentration distribution of NO appears along the primary vortex in the street canyon. NO concentration increases as building length increases because the wind is converged to the center of the street canyon. The maximum concentration of NO is 171 ppbv, 250 ppbv, 392 ppbv, and 829 ppbv, respectively. Also, NO concentration at the leeward side is higher than at windward side near the bottom because of the reverse flows. In the case of CTRL and Exp_L1, the highest concentration of NO located around the center of the street canyon in the lower layer because the wind blows outward near the bottom. In the case of CTRL, Exp_L1, and Exp_L2, NO concentration is affected by the center of vortex in the upper layer. In the case of Exp_L2 and Exp_L3, the highest concentration of NO locates at the leeward side, because the reverse flows become stronger by the double-eddy circulation around the both sides of the downwind building (Figs. 11c and 11d). In the case of Exp_L3, the highest concentration of NO appears near the bottom and around the upward building, because the flows converge at the center of the street canyon due to the double-eddy circulation. Figure 12

shows NO_2 concentration fields with the change of building length. The concentration distribution of NO_2 appears to be similar that of NO, but maximum concentration of NO_2 is lower than that of NO.

Figure 13 shows O_3 concentration fields with the change of building length. O_3 concentration around the downward building wall is higher than around the upward building wall, because O_3 is entrained into the canyon along the downward building wall in the rooftop level. O_3 concentration decreases as building length increases. In the case of CTRL, Exp_L1, and Exp_L2, O_3 concentration is lowest at the center of vortex because NO concentration is high at the center of the vortex. In the case of Exp_H3, the lowest concentration of O_3 is shown near the bottom and the upward building wall because O_3 concentration is depleted by the NO.

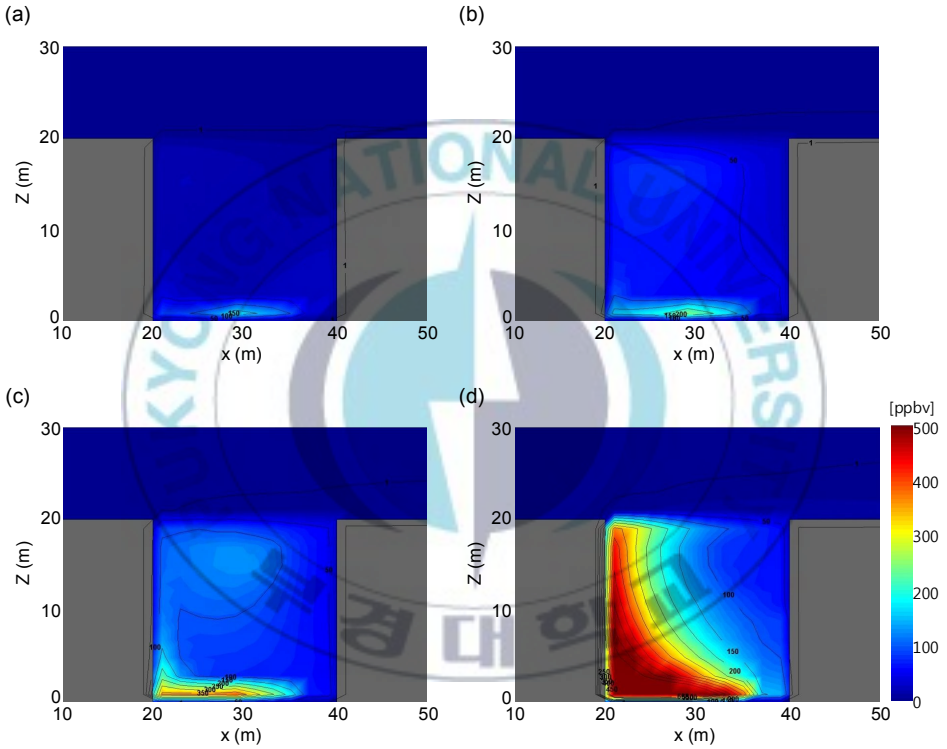

Fig. 11. NO concentration fields along the street canyon axis in the case of (a) CTRL case, (b) Exp_L1 case, (c) Exp_L2 case and (d) Exp_L3 case.

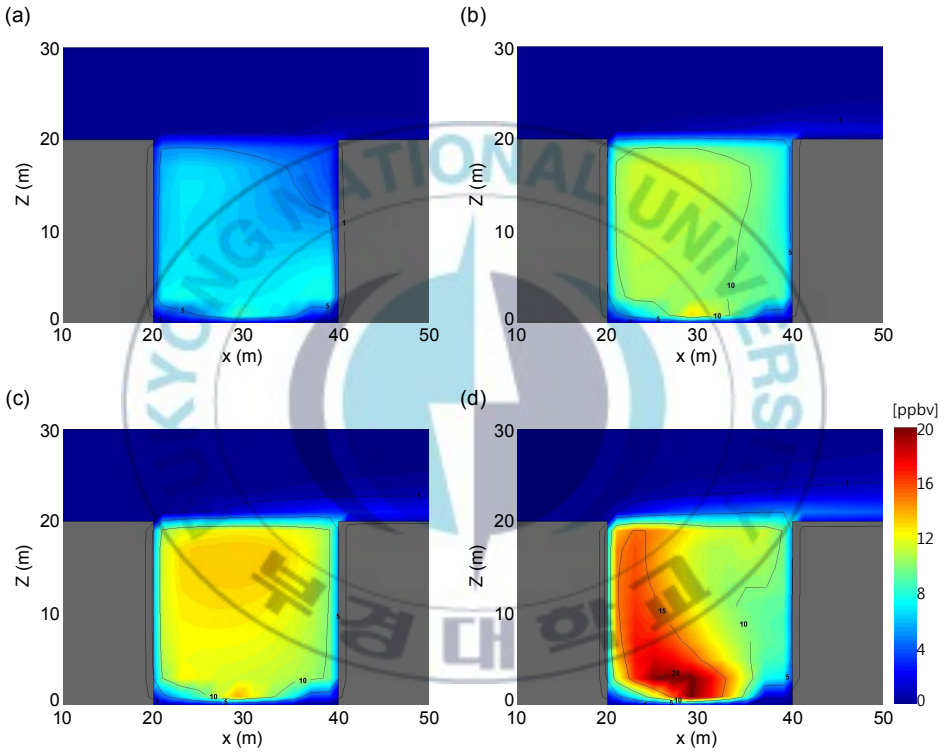

Fig. 12. NO_2 concentration fields along the street canyon axis in the case of (a) CTRL case, (b) Exp_L1 case, (c) Exp_L2 case and (d) Exp_L3 case.

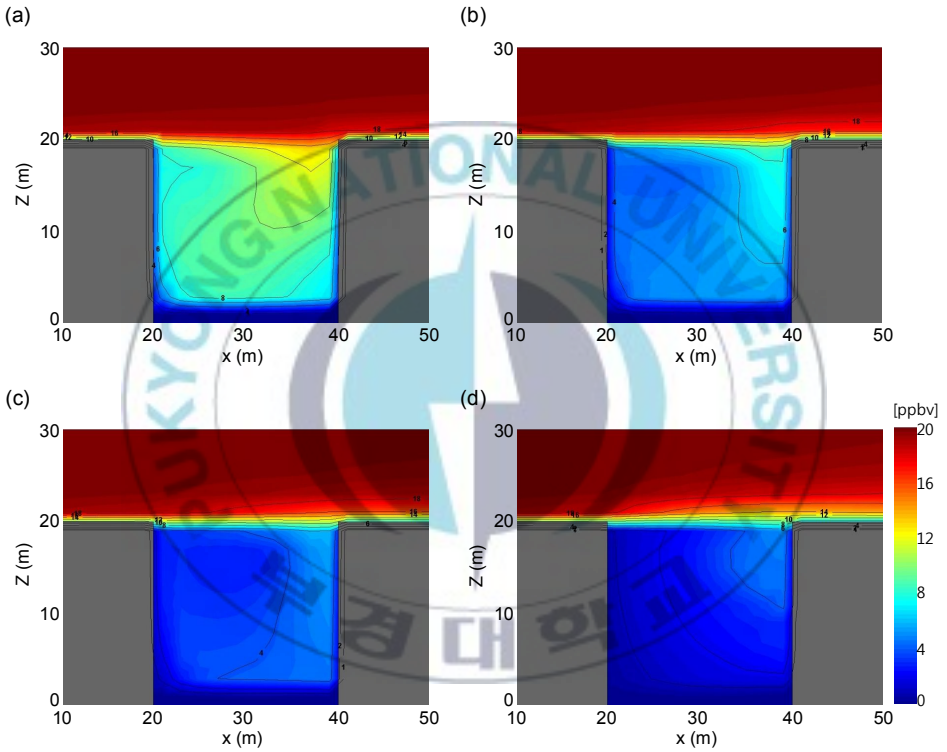

Fig. 13. O_3 concentration fields along the street canyon axis in the case of (a) CTRL case, (b) Exp_L1 case, (c) Exp_L2 case and (d) Exp_L3 case.

Figure 14 shows the average concentration of NO, NO_2, and O_3 at the bottom and at the whole street canyon with the change of building length. NO and NO_2 concentrations are the highest in Exp_L3 case, Exp_L2 case, Exp_L1 case, and CTRL case in sequence, but NO_2 concentration is almost uniform. The average concentration of O_3 at the bottom with the increase of building length decreases (5.4 ppbv, 2.8 ppbv, 2.0 ppbv, and 1.6 ppbv, respectively). O_3 concentration is the lowest as NO concentration is the highest in the case of Exp_L3. It is reconfirm that the pattern of O_3 concentration is contrasted with that of NO and NO_2 concentrations.

Figure 15 shows the average concentration of NO, NO_2, and O_3 at the leeward side and at the windward side with the change of building length. The leeward side expresses the area from upward building wall to the center of canyon. The windward side expresses the area from the center of canyon to downward side wall. The average concentration of NO and NO_2 increases as building length increases. NO and NO_2 concentrations at the leeward side are higher than at the windward side. The difference of NO concentration between at the leeward side and at the windward side increases as building length increases except CTRL case. In contrast to the concentration of NO, the difference of NO_2 concentration between at the leeward side and at the windward side decreases as building length increases. O_3 concentration decreases as building length

increases both at the leeward side and at the windward side. The average concentration of O_3 at the leeward side is lower than at the windward side.

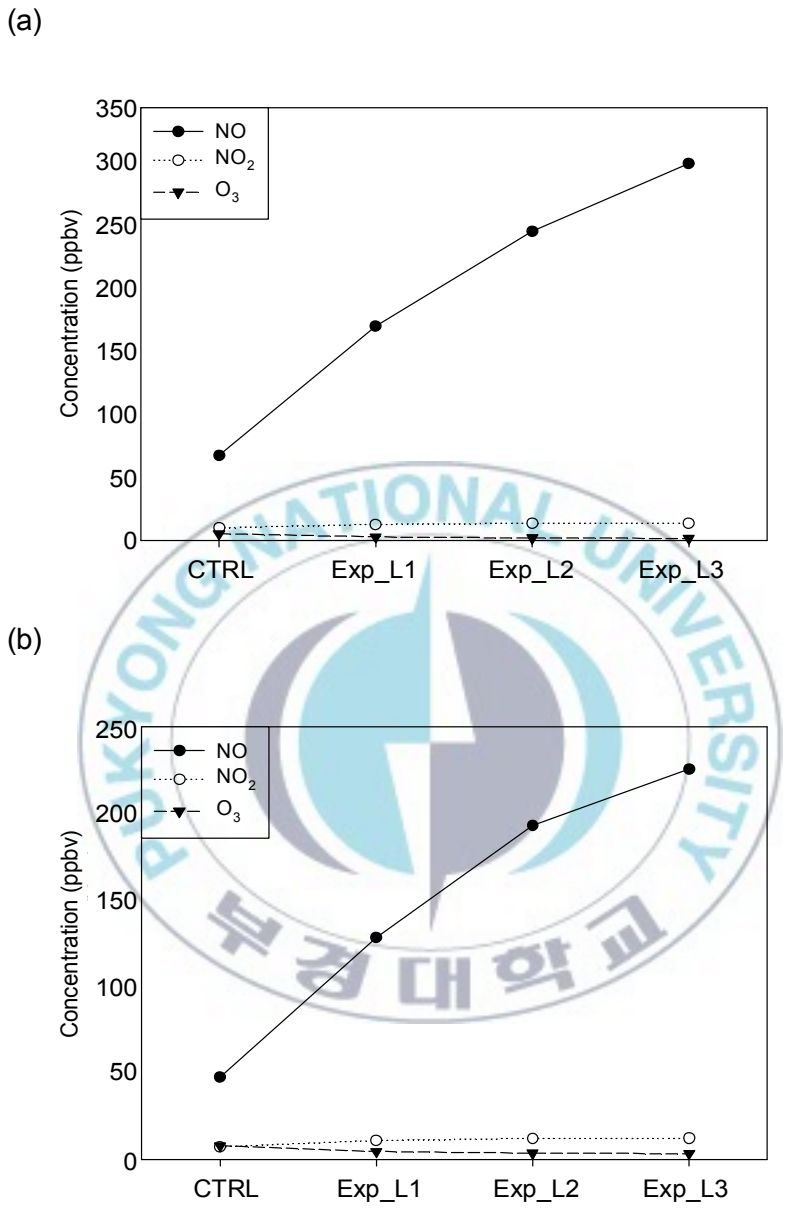

Fig. 14. The mean concentration of NO, NO_2 and O_3 (a) near the bottom in the street canyon and (b) at the whole street canyon with the change of building length.

(a)

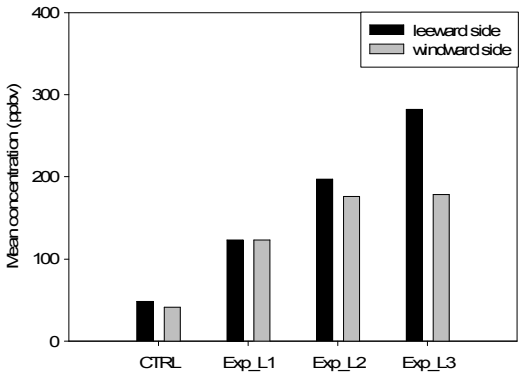

(b)

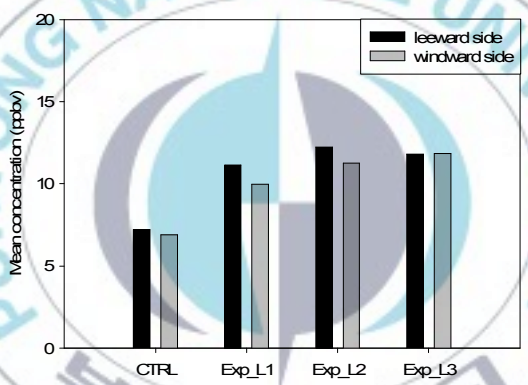

(c)

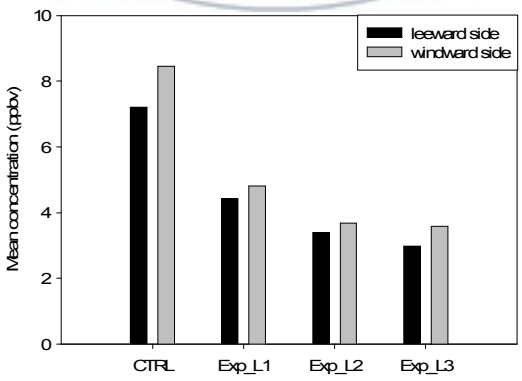

Fig. 15. The mean concentration of (a) NO, (b) NO_2, and (c) O_3 at the leeward side and at the windward side with the change of building length.

3. The effects of Street width

Figure 16 shows the fields of horizontal wind vectors in the street canyon with the change of street width (= 20 m, 30 m, 40 m, 50 m). In all the four cases with street width, the reverse flows appear near the bottom because one clockwise-rotating vortex is generated in the street canyon. The wind blows upward and outward around the upwind building in the lower layer. The wind blows downward and outward around the downwind building. The intensity of outward flows around the downward building in the street canyon increases as street width increase because the wind speeds decrease with the increase of street width in the streamwise (x-direction) street canyon. Wake interference flow occurs in the case of Exp_S2 and Exp_S3. Wake interference flow appears when the street canyon aspect ratio is 2 and the building aspect ratio is 1, according to the previous studies about the flow regime (Oke, 1988; Sini *et al.*, 1996). The wind blows downward and outward, and the double-eddy circulations behind the upwind building appear near the bottom (Figs. 16c and 16d). On the other hand, in the short street canyon, skimming flow effects on flow in the street canyon. In the long street canyon, wake interference flow effects on flow in the street canyon.

Figure 17 shows the fields of vertical wind vectors in the street

canyon. The vertical cross sections show that one clockwise-rotating vortex forms in the street canyon. The center of the vortex in the street canyon appears around the edges of upward building in the rooftop level. In the case of Exp_S3, the center of vortex is closer around the upward building than that of Exp_S2 case. The flow blows from downward building to upward building, reverse flows, appear near the bottom due to the clockwise-rotating vortex in the street canyon.

From the above results, it is ascertain to the various flow patterns appear as the change of street width. The change of street width effects on the flow pattern in the street canyon by the flow regime and the center of vertical vortex.

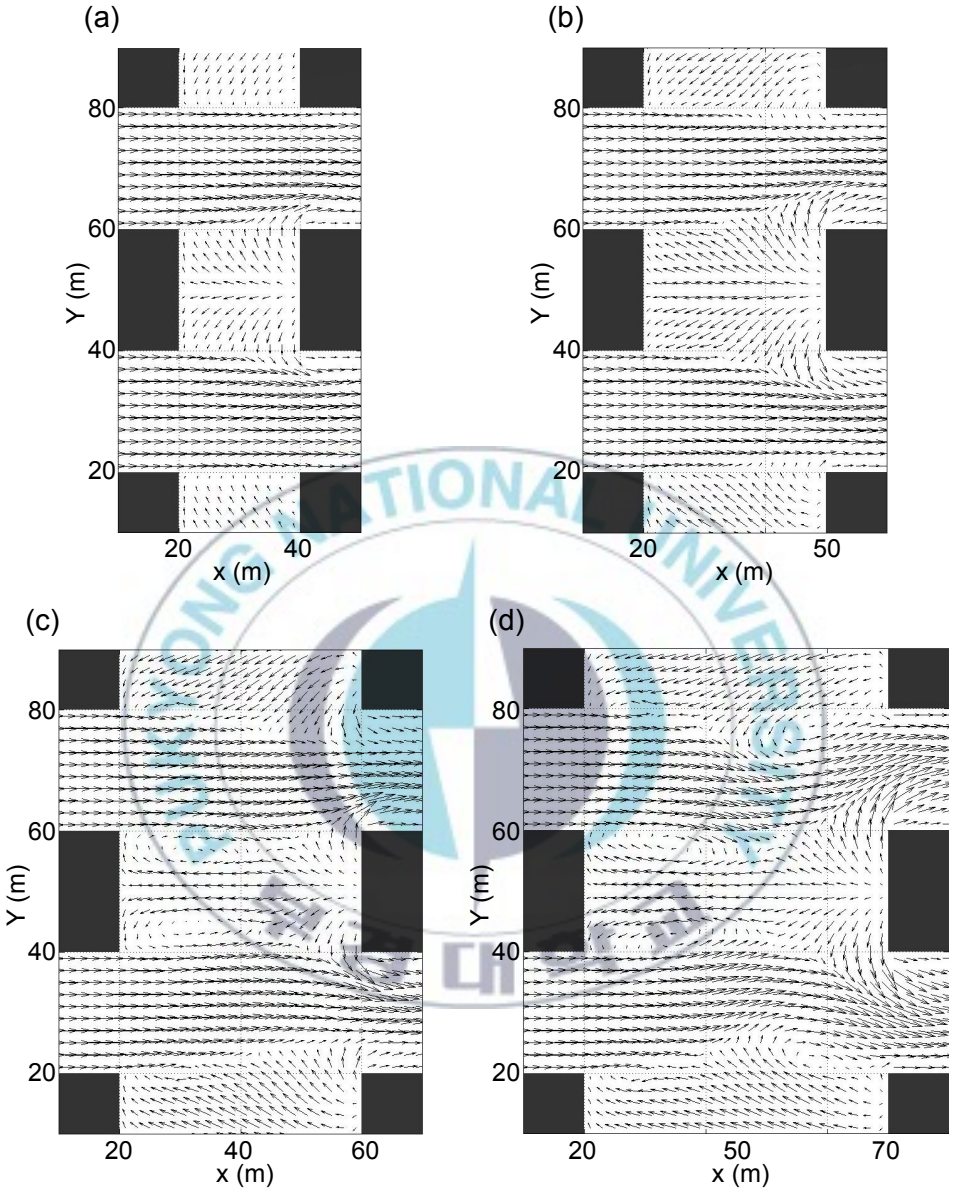

Fig. 16. The fields of horizontal wind vector at h = 1 m in the case of (a) CTRL case, (b) Exp_S1 case, (c) Exp_S2 case and (d) Exp_S3 case.

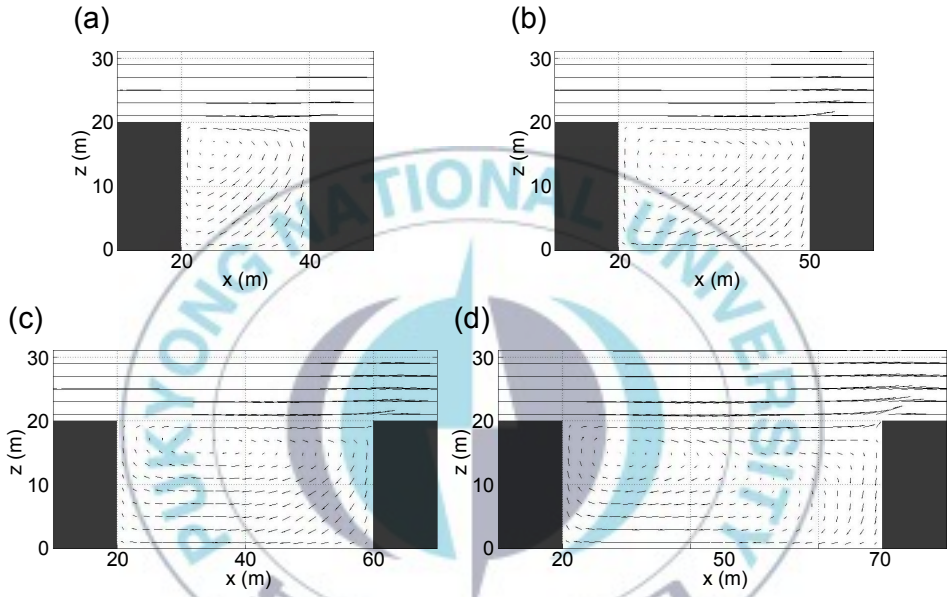

Fig. 17. The fields of vertical wind vector in the case of (a) CTRL case, (b) Exp_S1 case, (c) Exp_S2 case and (d) Exp_S3 case.

Four numerical simulations are performed with the change of street width and the simulation results for the dispersion of the reactive pollutant are analyzed. Figure 18 and 19 shows NO and NO_2 concentration fields with the change of street width, respectively. In all the four cases with the change of street width, NO and NO_2 concentrations at the leeward side is higher than at windward side because of the reverse flows near the bottom and the clockwise-rotating vortex in the street canyon. Also, the highest concentration of NO and NO_2 located around the center of the street canyon near the bottom. The maximum concentration of NO in CTRL case and Exp_S1 case is 171 ppbv and 147 ppbv at the center of the street canyon, respectively. However, the maximum concentration of NO in Exp_S2 and Exp_S3 is 220 ppbv and 202 ppbv, respectively. NO and NO_2 concentrations in the case of Exp_S2 and Exp_S3 are higher than in the case of CTRL and Exp_S1 because of the double-eddy circulation behind the upward building. The double-eddy circulation behind the upward building interrupts the outward flow and it leads to the higher NO and NO_2 concentrations behind upward building. On the other hand, the increasing street width decreases the concentration of NO and NO_2, but the existence of the double-eddy circulation in the street canyon increases the concentration of NO and NO_2. Figure 20 shows O_3 concentration fields with the change of street width. In the case of Exp_S1, Exp_S2, and Exp_S3, NO and NO_2 are entrained into the

outer edge of the primary vortex over the surface while O_3 is entrained into the street canyon. O_3 concentration around the downward building wall increases as street width increases. O_3 concentration around the upward building wall is lower than around the downward building because of chemical reaction of NO and O_3. It is shown that the concentration distribution of O_3 appear in contrasted with that of NO and NO_2.

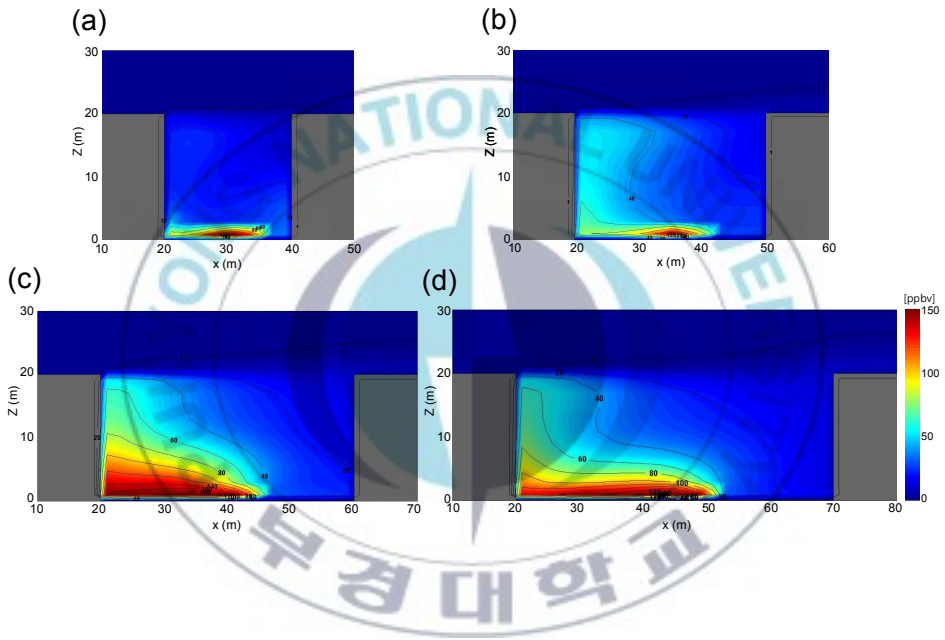

Fig. 18. NO concentration fields along the street canyon axis in the case of (a) CTRL case, (b) Exp_S1 case, (c) Exp_S2 case and (d) Exp_S3 case.

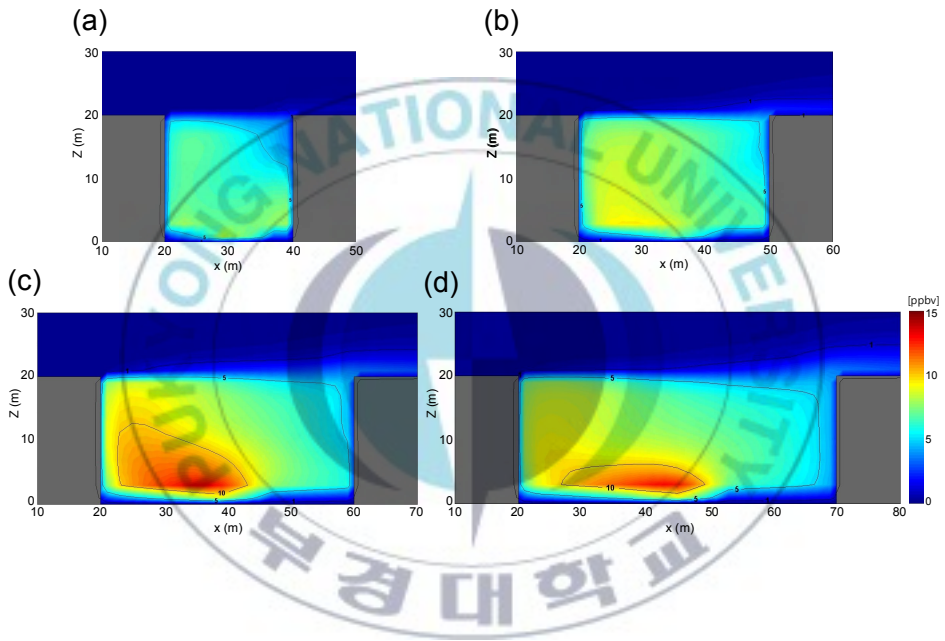

Fig. 19. NO_2 concentration fields along the street canyon axis in the case of (a) CTRL case, (b) Exp_S1 case, (c) Exp_S2 case and (d) Exp_S3 case.

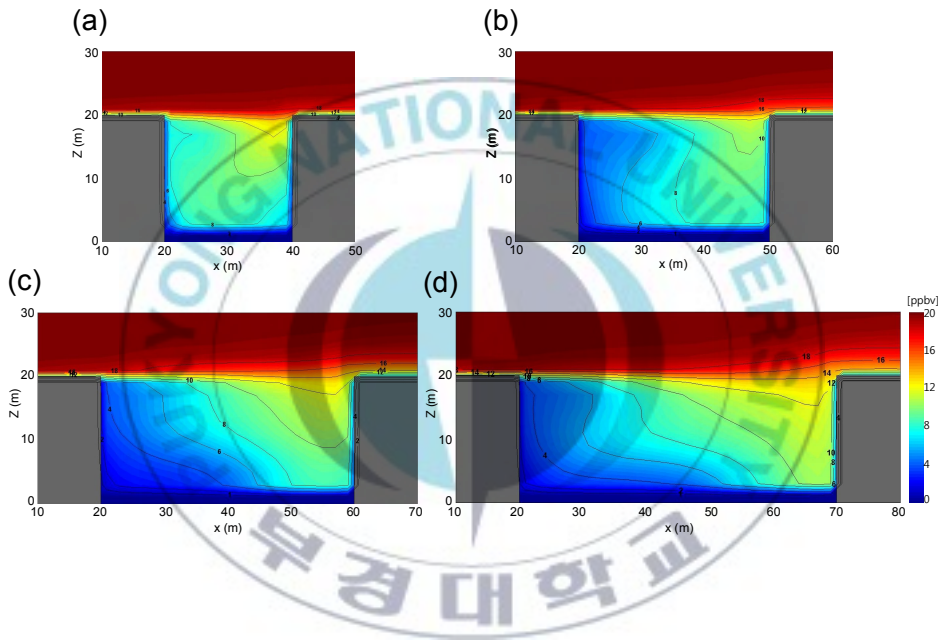

Fig. 20. O_3 concentration fields along the street canyon axis in the case of (a) CTRL case, (b) Exp_S1 case, (c) Exp_S2 case and (d) Exp_S3 case.

Figure 21 shows the average concentration of NO, NO_2, and O_3 at the bottom and at the whole street canyon with the change of street width. The average concentration at the bottom and at the whole street canyon considers area and volume for each cases, respectively. The pattern of NO and NO_2 concentration is divided by flow regime. NO concentration decreases with the increase of street width as the double-eddy circulations behind upward building do not exist (skimming flow). Also, NO concentration decreases as the double-eddy circulations exist behind upward building (wake interference flow). In the case of CTRL and Exp_S1 (skimming flow), the average concentration of NO increases as street width increases. In the case of Exp_S2 and Exp_S3 (wake interference flow), the average concentration of NO decreases as street width increases. However, the average concentration of NO_2 is almost uniform. In the case of Exp_S2 and Exp_S3, the average concentration of NO is higher than that of CTRL and Exp_S1 because of the double-eddy circulations behind upward building. The average concentration of O_3 is the lowest as NO concentration is the highest in the case of the Exp_S2. The average concentration O_3 decreases as street width increases with skimming flow. The average concentration O_3 increases as street width increases with wake interference flow.

Figure 22 shows the average concentration of NO, NO_2, and O_3 at the leeward side and at the windward side with the change of

street width. The leeward side expresses from upward building wall to the center of canyon. The windward side expresses from the center of canyon to downward side wall. Also, the average concentration consider the volume for each cases. In the leeward side, the average concentration of NO and NO_2 increases as street width increases with skimming flow. The average concentration of NO and NO_2 decreases as street width increases with wake interference flow. At the windward side, the average concentration of NO and NO_2 decreases as street width increases. The average concentration O_3 is contrasted with that of NO and NO2 at the windward side and at leeward side.

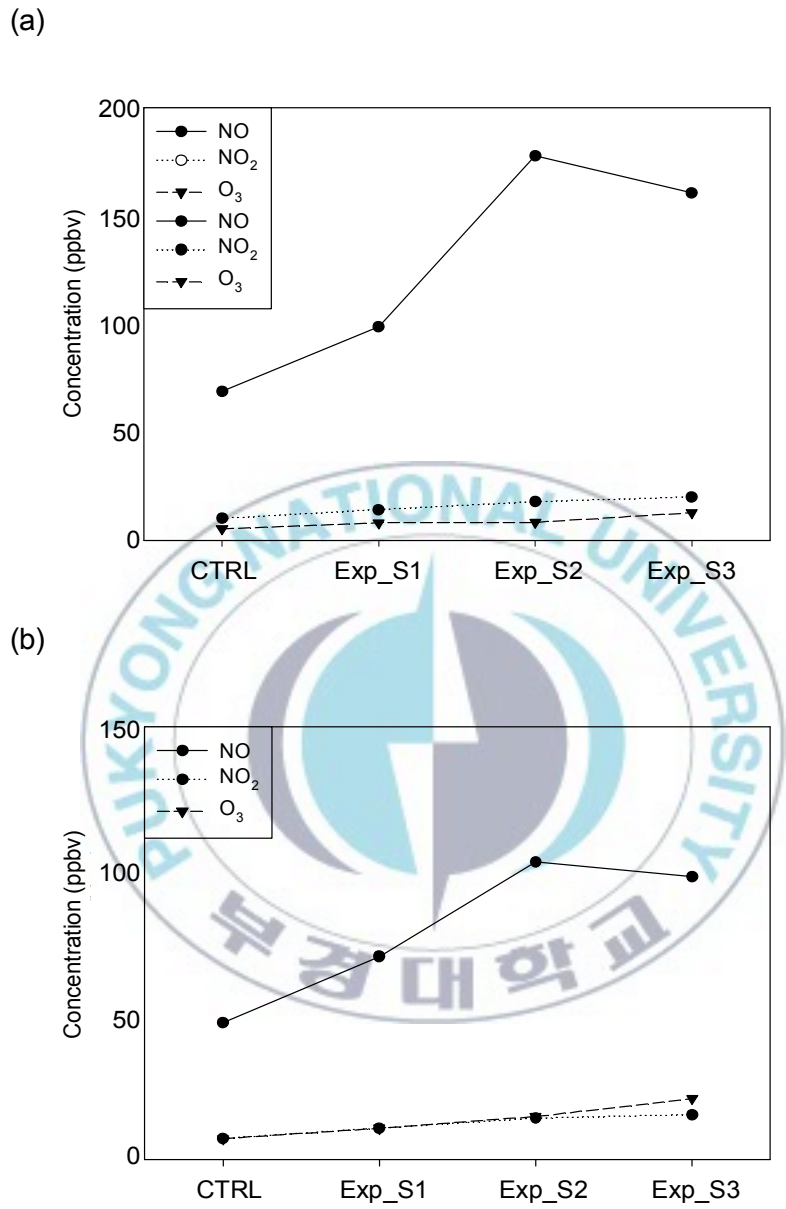

Fig. 21. The mean concentration of NO, NO_2 and O_3 (a) near the bottom in the street canyon and (b) at the whole street canyon with the change of street width.

(a)

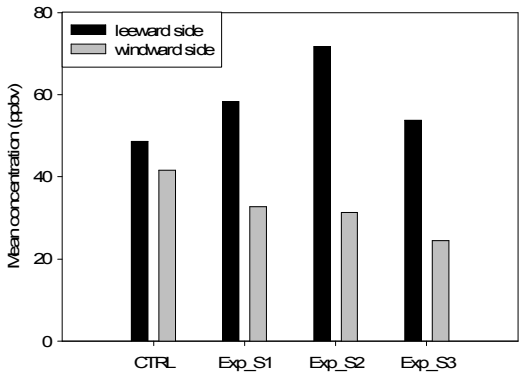

(b)

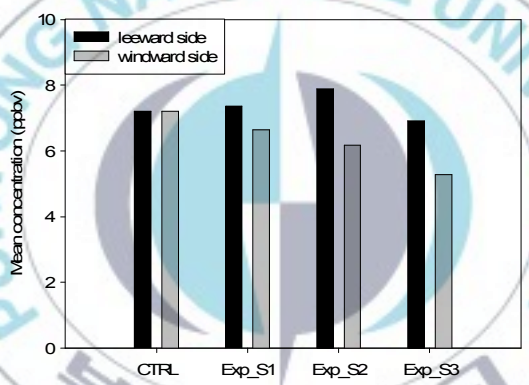

(c)

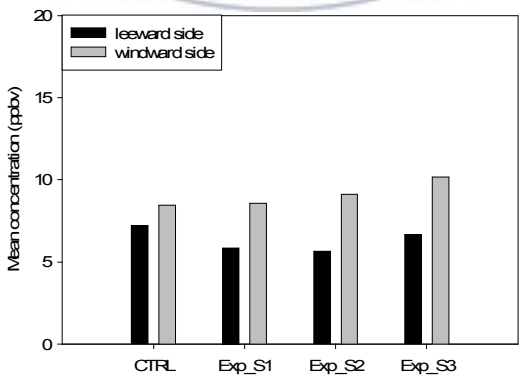

Fig. 22. The mean concentration of (a) NO, (b) NO_2, and (c) O_3 at the leeward side and at the windward side with the change of street width.

Ⅳ. Summary and Conclusion

In the daytime, the photochemical reaction by solar radiation effects on reactive pollutant dispersion. Also, the aspect ratio effects on flow and dispersion in urban street canyon. Many previous modeling studies was shown that the aspect ratio influence to the flow and dispersion in the street canyon. However, the most of previous studies considered the unreactive pollutant dispersion in microscale. In this study, the effects of aspect ratio on the flow and the reactive pollutant dispersion in urban street canyon are investigated using the CFD-Chem model. The model domain assume that the group of building repeated infinitely in x- and y-direction.

In the change of building height, vertical vortex effects on the flow in the street canyon. One vortex in the street canyon increases the concentration of NO and NO_2 near the bottom at the leeward side. Two counter-rotating vortex increases the concentration of NO and NO_2 near the bottom at the windward side. As the secondary vortex exists, NO and NO_2 concentrations is highest in the street canyon. In contrasted with NO and NO_2 concentration, the lowest O_3 concentration appears as the secondary vortex exists in the lower layer.

In the change of building length, the double-eddy circulation around the downward building effects on the flow in the street canyon. NO and NO_2 concentrations increase as building length

increases. As the double-eddy circulation exists in the street canyon, NO and NO_2 concentrations is higher than that as the double-eddy circulation do not exists in the street canyon. O_3 concentration decreases as building length increases in opposition to NO and NO_2 concentration.

In the change of street width, flow regime effects on the flow in the street canyon. NO and NO_2 concentrations increase as street width increases with skimming flow. NO and NO_2 concentrations decrease as street width increases with wake interferences flow. The double-eddy circulation behind the upward building with wake interferences flow interrupts the outward flow and it increases the NO and NO_2 concentrations in the street canyon. O_3 concentration around the downward building wall increases as street width increases because O_3 is entrained into the canyon while NO and NO_2 are entrained around the upward building wall.

This study demonstrated that the flow generated by the aspect ratio in urban street canyon effects on NO and NO_2 concentrations distribution. Also, the distribution of NO and NO_2 effects on the distribution of O_3 because O_3 depleted by NO. It is concluded that the aspect ratio can affect the flow pattern and it lead to the change of the distribution of the reactive pollutant concentration.

References

Assimakopoulos, V.D., H.M. ApSimon, and N. Moussiopoulos, 2003: A numerical study of atmospheric pollutant dispersion in different two-dimensional street canyon configurations. *Atmospheric Environment,* **37**, 4037 - 4049.

Baik, J.J., Y.S. Kang, and J.J. Kim, 2007: Modeling reactive pollutant dispersion in an urban street canyon. *Atmospheric Environment,* **41**, 934 - 949.

_____, S.B. Park, and J.J. Kim, 2009: Urban flow and dispersion simulation using a CFD model coupled to a mesoscale model. *Jounal of applied Meteorology and Climatology,* **48**, 1667 - 1681.

Baker, J., H.L Walker, and X. Cai, 2004: A study of the dispersion and transport of reactive pollutants in and above street canyon - a large eddy simulation. *Atmospheric Environment,* **38**, 6883 - 6892.

Bey, I., D.J. Jacob, R.M. Yantosca, J.A. Logan, B.D. Field, A.M. Fiore, Q. Li, H.Y. Liu, L.J. Mickley, and M.G. Schultz, 2001: Global modeling of tropospheric chemistry with assimilated meteorology: Model description and evaluation. *Journal of Geophysical Research,* **106**, 23073 - 23095.

Castro, I. P., and D.D. Apsley, 1997: Flow and dispersion over topography: a comparison between numerical and laboratory data for two-dimensional flow. *Atmospheric Environment*, **31**, 893-850.

Chan, T.L., G. Dong, C.W. Leung, C.S. Cheung, and W.T. Hung, 2002: Validation of a two-dimensional pollutant dispersion model in an isolated street canyon. *Atmospheric Environment,* **36**, 861 - 872.

Cheng, C.H., and R.N. Meroney, 2003: Concentration and flow distributions in urban street canyons: wind tunnel and computational data. *Journal of Wind Engineering,* **91**, 1141 - 1154.

Garmory, A., I.S. Kim, R.E. Britter, and E. Mastorakos, 2009: Simulations of the dispersion of reactive pollutants in a street canyon, considering different chemical mechanisms and micromixing. *Atmospheric Environment,* **43**, 4670 - 4680.

Jacobson, M.Z., and R.P. Turco, 1994: SMVGEAR: A sparse-matrix, vectorized gear code for atmospheric models. *Atmospheric Environment,* **28**, 273 - 284.

Kang, Y.S., J.J. Baik, and J.J. Kim, 2008: Further studies of flow and reactive pollutant dispersion in a street canyon with bottom heating. *Atmospheric Environment,* **42**, 4964 - 4975.

Kikumoto, H., and R. Ooka, 2012: A numerical study of air pollutant dispersion with bimolecular chemical reactions in an urban street canyon using large-eddy simulation. *Atmospheric Environment,* **54**, 456 - 464.

Kim, D.Y., A. Kondo, S. Soda, J.H. Oh, and K.M. Lee, 2008: Sensitivity analysis of primary pollutants on generationg photochemical oxidants over the Osaka Bay and its surrounding areas of Japan. *Journal of applied Meteorology Society of Japan,* **86**, 883 - 899.

Kim, J.J., and J.J. Baik, 2004: A numerical study of the effects of ambient wind direction on flow and dispersion in urban street canyon using the RNG κ-ε turbulence model. *Atmospheric Environment,* **38**, 3039 - 3048.

Kim, M.J., R.J. Park, and J.J. Kim, 2012: Urban air quality modeling with fill O_3-NO_x-VOC chemistry: Implications for O_3 and PM air quality in a street canyon. *Atmospheric Environment,* **47**, 330 - 340.

Kwak, K.H., and J.J. Baik, 2012: A CFD modeling study of the impacts of NO_x and VOC emissions on reactive pollutant dispersion in and above a street canyon. *Atmospheric Environment,* **46**, 71 - 80.

Li, X.X., C.H. Liu, and D.Y.C. Leung, 2008: Large-eddy simulation of flow and pollutant dispersion in high-aspect-ratio urban street canyons with wall model. *Boundary-Layer Meteorology,* **129**, 249 - 268.

Lin, S.J., and R.B. Rood, 1996: Multidimensional flux-form semi-lagrangian transport schemes. *Monthly Weather Review,* **124**, 2046 - 2070.

Liu, C.H., and M.C. Barth, 2002: Large-eddy simulation of flow and scalar transport in a modeled street canyon. *Journal of applied Meteorology,* **41**, 660 - 673.

_____, _____, and D.Y.C. Leung, 2004: Large-eddy simulation of flow and pollutant transport in street canyon of different building-height-to-street-width ratios. *Journal of applied Meteorology,* **43**, 1410 - 1424.

Mukherjee, P., and S. Viswanathan, 2001: Carbon monoxide modeling from transportation sources. *Chemosphere,* **45**, 1071 - 1083.

Oke, T. R., 1988: Street design and urban canopy layer climate. *Energy and Building*, **11**, 103 - 113.

Park, S.K., S.D. Kim, and H.W. Lee, 2004: Dispersion characteristics of vehicle emission in an urban street canyon. *Science of the Total Environment,* **323**, 263 - 271.

Tutar, M., and G. Oguz, 2002: Large eddy simulation of wind flow around parallel buildings with varying configurations. *Fluid Dynamics Research,* **31**, 289 - 315.

Sagrado, A.P.G., J. Beeck, P. Rambaud, and D. Olivari, 2002: Numerical and experimental modelling of pollutant dispersion in a street canyon. *Atmospheric Environment,* **90**, 321 - 339.

Sini, J.-F., S. Anquetin, and P. G. Mestayer, 1996: Pollutant dispersion and thermal effects in urban street canyons. *Atmospheric Environment*, **30**, 2659 - 2677.

Wild, O., X. Zhu, M.J. Prather, 2000: Fast-J: Accurate simulation of in- and below-cloud photolysis in tropospheric chemical models. *Journal of Atmospheric Chemistry,* **37**, 245 - 282.

Wu, S., L.J. Mickley, D.J. Jacob, J.A. Logan, R.M. Yantosca, and D. Rind, 2007: Why are there large differences between models in global budgets of tropospheric ozone?. *Journal of Geophysical Research,* **112**, D05302, doi:10.1029/2006JD007801.

Yakhot, V., S.A. Orszag, S. Thangam, T.B. Gatski, and C.G. Speziable, 1992: Development of turbulence models for shear flow by a double expansion technique, *Physics of Fluids* A, **4**, 1510-1520.